

Nonlinear rheology of dense colloidal systems with short-ranged attraction: A mode-coupling theory analysis

Madhu Priya¹ and Thomas Voigtmann^{1,2}

¹*Institut für Materialphysik im Weltraum, Deutsches Zentrum für Luft- und Raumfahrt (DLR), 51170 Köln, Germany*

²*Zukunftskolleg and Fachbereich Physik, Universität Konstanz, 78457 Konstanz, Germany*

(Dated: May 19, 2018)

The nonlinear rheology of glass-forming colloidal suspensions with short-ranged attractions is discussed within the integration-through transients framework combined with the mode-coupling theory of the glass transition (ITT-MCT). Calculations are based on the square-well system (SWS), as a model for colloid-polymer mixtures. The high-density regime featuring reentrant melting of the glass upon increasing the attraction strength, and the crossover from repulsive glasses formed at weak attraction to attractive glasses formed at strong attraction, are discussed. Flow curves are found in qualitative agreement with experimental data, featuring a strong increase in the yield stress, and, for suitable interaction parameters, the crossover between two yield stresses. The yield strain, defined as the position of the stress overshoot under startup flow, is found to be proportional to the attraction range for strong attraction. At weak and intermediate attraction strength, the combined effects of hard-core caging and attraction-driven bonding result in a richer dependence on the parameters. The first normal-stress difference exhibits a weaker dependence on short-ranged attractions as the shear stress, since the latter is more sensitive to the short-wavelength features of the static structure.

I. INTRODUCTION

The ability to fine-tune the rheological properties of colloidal suspensions is of large importance in manufacturing, in particular of high-solid dispersions ([1]). A reduction in viscosity at constant solid loading helps to flow these systems more efficiently; this is typically achieved by adding smaller particles or controlling the particle-size polydispersity (as first detailed in rheological context by Farris [2]), be it in ceramic processing ([3]) or in food rheology ([4]).

Another way of adjusting the viscosity of highly dense hard-particle suspensions is to make use of effective attractive interactions among the colloids ([5–7]). In charge-stabilized suspensions of nearly hard-sphere particles, such attractions can be fine-tuned by adding nonadsorbing polymers to the solution. This has recently been described by Willenbacher *et al.* [8] for technologically relevant aqueous dispersions of polystyrene-microgel and latex particles. Adding a few g/l of a linear polyethylene-oxide polymer resulted in a reduction in viscosity by up to two orders of magnitude.

This procedure makes use of a depletion-attraction-induced reentrant behavior of the glass transition in the colloid-density-attraction-strength state space. It is well known that the addition of free polymer to a hard-sphere like colloidal suspension induces an entropic interaction among them: around the colloid particles, a depletion layer deprived of polymer exists, but on approach, two colloid particles can reduce the total volume of this layer, resulting in an entropic gain for the distribution of the polymer coils. If the polymer is treated as ideal-gas like, the resulting effective interaction among the colloids is well described by the Asakura-Oosawa potential ([9]). For the purpose of a qualitative discussion, a simpler model system is the square-well system (SWS), where one

simply assumes, relative to the hard-sphere diameter d , a constant attraction of width δ (set by the radius of gyration of the free polymer) and strength U_0 (controlled by the polymer concentration) surrounding the hard-sphere core of the colloid. Together with the colloid packing fraction φ , and normalizing energies by those of thermal fluctuations, $\Gamma = U_0/k_B T$, the three control parameters of the SWS thus are $(\varphi, \Gamma, \delta)$.

The SWS model at high density allows to distinguish repulsion-driven glasses for small Γ , from attraction-driven glasses for large Γ . This distinction was first established as a qualitative one in the mode-coupling theory of the glass transition (MCT) ([10–12]), where for small enough attraction range, it is signalled by a glass-glass transition. Crossing this transition, the nonergodic contribution to the average structure of the amorphous solid changes abruptly, leading to a sharp change in elastic moduli and related quantities. The glass-glass transition results from a crossing of glass-transition lines in the Γ - φ plane, one leading to the “repulsive glass” (weakly dependent on Γ), the other leading to the “attractive glass” (depending more strongly on Γ than on φ). The repulsive glass is characterized by hard-core repulsion, and particles are localized since they are trapped in “cages” formed by their neighbors. As a result, individual-particle motion becomes localized at the repulsive-glass transition on a length scale of typically around 10% of a particle diameter. This is often referred to as the criterion of Lindemann (who estimated a similar localization length close to the melting point of crystals). In the attractive glass on the other hand, particle localization is driven by “bonds” formed between the particles, leading to a localization length of the order of δ . If $\delta \ll 0.1$, the two arrest mechanisms occur on separated length scales, leading to rich dynamical behavior in the parameter regime where both transition lines meet. In particular, MCT

predicts a critical attraction range, $\delta^* \approx 0.0465$ ([12]), where a higher-order bifurcation singularity in the glass-transition diagram appears. For $\delta < \delta^*$, the glass-glass transition emerges, whose endpoint is also connected to a higher-order singularity. These influence the dynamics in the vicinity: the well documented two-step relaxation process of density fluctuations close to the ordinary glass transition is replaced by leading-order asymptotic logarithmic decay ([13, 14]).

En route to the attractive glass, a weak attraction is found to destabilize the repulsive glass, shifting its transition point to higher packing fraction. This is thought to arise since the attraction-induced increase of particle pairs in close contact inevitably opens up nearest-neighbor cages ([15]). As a result, one can find lines through the state space, say at fixed packing fraction φ and polymer size ratio δ , where a continuous increase in attraction strength first melts the repulsive glass, and then re-freezes the resulting liquid as an attractive glass. This “reentry phenomenon” is the basis of the viscosity reduction discussed by Willenbacher *et al.* [8].

The predictions of MCT for the quiescent dynamics of the high-density SWS have been extensively tested in simulation ([16]) and experiment ([17–19]). The theory gives a good qualitative account of the phenomena there, although especially in the attractive glass, certain hopping-like relaxation modes that destroy bonding-induced particle localization are not accounted for in MCT.

Since the attractive glass lines extends to low φ , it is tempting to connect this low-density attractive-glass transition predicted by MCT with the gel transition, and several studies address the low-density limit ([11, 20–23]). However, gelation involves spatial heterogeneities outside the scope of MCT, so a subtle distinction between (low-density) gels and (high-density) attractive glasses has to be maintained ([24–30]). Numerous of rheology studies have discussed gelation-induced phenomena in detail (see, e.g., Rueb and Zukoski [31], Prasad *et al.* [32], and Lindström *et al.* [33] and references therein). Only more recently, the high-density attractive-glass regime has caught attention. We restrict ourselves to this regime in the following.

The rheological signature of the reentrant glass transition in the SWS, but also in related binary mixtures of particles with very different sizes, in terms of linear-response shear moduli has been discussed before ([34–38]). Since the relevant length scale changes, one notes a strong increase with increasing attraction, from values $\sim k_B T/d^3$ (where d is the colloid diameter), to values $\sim k_B T/d^3/\delta$ (if the attraction strength is kept constant) ([21]).

An intriguing phenomenon arising in the nonlinear rheology of attractive glasses was first pointed out in seminal papers by Pham *et al.* [39, 40]. Using strain sweeps of large-amplitude oscillatory rheology, they found a two-step yielding, indicated by two distinct peaks in the stress-strain-amplitude curves: the first emerges at the

end of the reversible (almost) linear response regime at around $\gamma_y \approx 10\%$ of strain amplitude, while the second appears at much higher amplitudes, (50% to 100% in their study). The first peak is reminiscent of the yielding of hard-sphere repulsive glasses: there, stress-strain curves typically show a nonmonotonic crossover between the (almost) linear elastic-like increase at low strain to the steady-state stress approached in the flowing state. This “stress overshoot” ([41–43]) is interpreted as the point where nearest-neighbor cages first break, in agreement with its position γ_y and the Lindemann criterion. One indeed observes that the first yielding step occurs at lower γ_y for lower δ ([30]). The second peak observed in attractive glasses is now generally interpreted as the breakup of larger structural units (such as clusters) ([29]) that can still form even if individual bonds are broken.

Theoretical descriptions of the yielding behavior of attractive glasses are still scarce. Notably, Kobelev and Schweizer [44, 45] were the first to address the limit of attractions strong compared to thermal fluctuations, using the notion of barrier crossing in a nonequilibrium free-energy landscape that is modified by shear.

MCT has been extended to describe the nonlinear rheology of shear-thinning colloidal suspensions by Fuchs and Cates ([46–48]), in a framework called integration through transients (ITT). This theory starts from the nonequilibrium Smoluchowski equation and contains coupling coefficients that are given in terms of the equilibrium static structure functions. Its application to the SWS is hence straightforward, but lacking so far. In this contribution, we employ the ITT-MCT with an additional isotropic assumption for its memory function, to the SWS model studied previously in the quiescent state. We specifically address the flow curves in the vicinity of the glass-glass transition, and discuss the dependence of the ITT-MCT yield strain on attraction range δ and strength Γ .

The paper is organized as follows: in Sec. II we outline the theory together with technical details of the calculation. In Sec. III we present results for flowcurves and stress-strain relations, followed by a discussion of the results in light of experimental findings (Sec. IV). Section V contains conclusions.

II. THEORY

The ITT-MCT description of nonlinear rheology of glass-forming colloidal suspensions is based around transient correlation functions, in particular those of colloid number-density fluctuations of the N -particle system, $\varrho_{\vec{q}} = \sum_{k=1}^N \exp[i\vec{q} \cdot \vec{r}_k]$. In the case of an imposed time-independent shear rate, the transient density correlator $\phi_{\vec{q}}(t) = \langle \varrho_{\vec{q}}^* \exp[\Omega^\dagger t] \varrho_{\vec{q}(t)} \rangle / \mathcal{N}$ measures the overlap of a density fluctuation at wave-vector \vec{q} with one at a time t earlier whose wavevector $\vec{q}(t)$ evolves due to flow-induced advection to become \vec{q} . Here, Ω^\dagger is the adjoint Smoluchowski operator describing the time evolution of dynam-

ical variables of the colloidal system, i.e., the Brownian motion of N interacting particles on top of the prescribed flow field. Hydrodynamic interactions are neglected in the theory. The angular brackets denote the canonical equilibrium average, and \mathcal{N} is a normalization factor to set $\phi_{\vec{q}}(0) = 1$.

In principle, the wave-vector dependent correlation functions under flow are anisotropic. However, structural anisotropies of sheared dense colloidal suspensions are found to be rather small ([42, 49]), at least at small bare Péclet numbers, $\dot{\gamma}\tau_0 \ll 1$, with the Brownian relaxation time of a single particle τ_0 . One can hence consider an ad-hoc simplification of ITT-MCT where the wave-vector dependence of all correlation functions is assumed to be isotropic. This approximation was first applied to discuss the qualitative features of the hard-sphere system under shear, where it was termed the isotropically sheared hard-sphere model (ISHSM) ([47, 50]). The full anisotropic ITT-MCT equations are numerically rather demanding and have been solved so far only in two spatial dimensions ([49]). Only very recently, the full 3D theory has been solved. This scheme has now also been applied to the SWS model ([51]), but only a selected number of state points for one particular attraction range could be studied. The attraction-induced sensitivity of the MCT integrals to a much larger wave-vector range as for hard spheres ([12]) makes it desirable to employ large numerical grids in the numerical evaluation of the theory. This is something that is not yet easily done in the full 3D anisotropic calculation. The present study hence employs the isotropic approximation, in order to provide a qualitative account of a wider parameter range. Comparing with Amann and Fuchs [51], the effects of the isotropization of the theory can be checked; they are found to be quantitative, but not qualitative.

The isotropic ITT-MCT equation of motion for the transient density correlation function in steady shear is given by

$$\dot{\phi}_q(t) + \Gamma_q \left\{ \phi_q(t) + \int_0^t dt' m_q(t-t') \dot{\phi}_q(t') \right\} = 0. \quad (1)$$

Here, $m_q(t)$ is the memory kernel describing the combined effects of slow structural relaxation and its modification through shear. In the isotropic model one sets

$$m_q(t) \approx \frac{1}{2V} S_q \sum_{\vec{k}} V_{\vec{q},\vec{k}}^{(\dot{\gamma})}(t) S_k S_p \phi_k(t) \phi_{|\vec{q}-\vec{k}|}(t), \quad (2)$$

with the mode-coupling vertex that is time dependent due to the advection in shear flow. This vertex is, as usual, determined by the equilibrium, quiescent direct correlation functions (DCF) c_k alone. The DCF is connected to the static structure factor of the system, $S_k = 1/(1 - nc_k)$, where n is the colloid number density. One has

$$V_{\vec{q},\vec{k}}^{(\dot{\gamma})}(t) = \frac{n}{q^4} \left[\vec{q} \cdot \vec{k} c_k(t) + \vec{q} \cdot \vec{p} c_p(t) \right] \left[\vec{q} \cdot \vec{k} c_k + \vec{q} \cdot \vec{p} c_p \right]. \quad (3)$$

Here, $k(t) = k\sqrt{1 + (\dot{\gamma}t/\gamma_c)^2/3}$ is the advected wave vector in the isotropic approximation. The dimensionless model parameter γ_c is included here, following a suggestion originally discussed in the schematic-model simplification of ITT-MCT ([52]), to adjust the scale of the repulsive-glass cage breaking. We fix this parameter to $\gamma_c = 0.1$, independent on density, attraction strength or width.

In the quiescent state, MCT predicts the long-time behavior of $\phi_q(t)$ to change at certain critical control parameters, identified as idealized glass transitions ([53]). For small enough coupling strength in the memory kernel, $\phi_q(t)$ decays to zero as expected for a liquid. For stronger coupling, a finite nonergodicity parameter (also called glass form factor), $f_q = \lim_{t \rightarrow \infty} \phi_q(t) > 0$, arises and signals dynamical arrest of density fluctuations. The f_q are determined by a set of nonlinear equations, and the transition points of MCT are bifurcation points of these equations. These ideal glass transitions can be classified into the simplest sequence of bifurcation transitions, termed \mathcal{A}_ℓ bifurcations with $\ell = 2, 3, \dots$ in the mathematical literature. The main contributions to the wave-vector dependent coupling of density correlators close to such \mathcal{A}_ℓ transitions stem from intermediate q . Wave-vector advection under shear decorrelates the contributions from the DCF appearing in the MCT vertices, Eq. (3), and hence counteracts dynamical arrest. This is the basis of shear thinning in ITT-MCT. It also implies that under steady shear, any finite shear rate will melt the glass ([46]).

To derive a nonlinear constitutive equation for the non-Newtonian stress tensor based on ITT-MCT, one starts from the full anisotropic nonlinear generalization of a Green-Kubo relation ([46, 54, 55]). In the isotropic approximation, one writes

$$\boldsymbol{\sigma}(t) = \int_0^t dt' \left[-\frac{\partial}{\partial t'} \mathbf{B}(t-t') \right] G(t-t'), \quad (4)$$

assuming time-independent shear to start at $t = 0$ from a stress-free equilibrium state. Here, the Finger tensor (or left Cauchy-Green tensor) appears,

$$\mathbf{B}(t-t') = \begin{pmatrix} 1 + \gamma_{tt'}^2 & \gamma_{tt'} & 0 \\ \gamma_{tt'} & 1 & 0 \\ 0 & 0 & 1 \end{pmatrix}, \quad (5)$$

for simple shear with a velocity gradient $\dot{\gamma} = \partial_y v_x$. The accumulated strain is given by $\gamma_{tt'} = \int_{t'}^t \dot{\gamma}(s) ds$, or simply $\dot{\gamma}(t-t')$ for steady shear. The Finger tensor ensures that Eq. (4) obeys the principle of material objectivity ([56]).

For the nonlinear dynamic shear modulus $G(t)$, different isotropic ITT-MCT approximations exist ([47]). In the following, we use the original proposition ([50]),

$$G(t) = \frac{k_B T}{60\pi^2} \int dk k^4 \frac{S'_k S'_{k(t)}}{S_{k(t)}^2} \phi_k^2(t), \quad (6)$$

which we find to give most consistent results overall. From Eqs. (4) and (6), one obtains the shear stress as

$$\sigma_{xy}(t) = \dot{\gamma} \int_0^t dt' G(t'). \quad (7)$$

We will denote the steady-state value of the shear stress by $\sigma = \lim_{t \rightarrow \infty} \sigma_{xy}(t)$. It is used to define the shear viscosity in the usual way, $\eta = \sigma/\dot{\gamma}$.

Equation (4) also allows to calculate normal-stress differences, $N_1 = \sigma_{xx} - \sigma_{yy}$ and $N_2 = \sigma_{yy} - \sigma_{zz}$. In the full anisotropic ITT-MCT, both a first and a second normal-stress difference appear ([51, 57]), but typically the latter is an order of magnitude smaller. In the isotropic model used here, the second normal-stress difference is identically zero, $N_2 = 0$. The first normal-stress difference is given by

$$N_1 = 2\dot{\gamma}^2 \int_0^\infty dt t G(t), \quad (8)$$

yielding the first normal-stress coefficient, $\Psi_1 = N_1/\dot{\gamma}^2$.

It is apparent from above that both the viscosity and the first normal-stress coefficient are given through very similar wave-number integrals, only differing by an additional factor t in the time integral for Ψ_1 . We define the corresponding wave-number dependent integrands I_η and I_{Ψ_1} to discuss the relevance of different contributions coming from different wave lengths, through $\eta = \int I_\eta(k) dk$ and $\Psi_1 = \int I_{\Psi_1}(k) dk$, following a similar definition proposed by Farage *et al.* [57]. Explicitly, in the isotropic ITT-MCT model,

$$I_\eta(k) = \int_0^\infty dt \frac{k_B T}{60\pi^2} k^4 \frac{S'_k S'_{k(t)}}{S_{k(t)}^2} \phi_k^2(t), \quad (9)$$

and

$$I_{\Psi_1}(k) = \int_0^\infty dt t \frac{k_B T}{60\pi^2} k^4 \frac{S'_k S'_{k(t)}}{S_{k(t)}^2} \phi_k^2(t). \quad (10)$$

The time dependence of the advected wave-vectors cause these expressions to display different features as function of k , as we will discuss further below.

Equations (1) to (3) are solved numerically using a standard procedure adapted to the calculation of slowly decaying correlation functions ([50]). From $\phi_q(t)$, one obtains $G(t)$ and hence $\sigma(t)$ as well as $N_1(t)$ by a simple integration using the trapezoidal rule. In solving the ITT-MCT equations numerically, one has to specify a discrete grid of wave vectors, including both a low- q and high- q cutoff. The latter has to be chosen large enough, since the DCF entering the MCT vertex will exhibit a slowly decaying power-law contribution, $c_q \sim \sin[qd(1 + \delta/2)]/q$ in a range $\pi \ll qd \ll \pi/\delta$, before crossing over to its true $1/q^2$ asymptote ([12]). Hence for small δ , the large- q structure of the vertex is decisive. We fix the upper wave-number cutoff to $Q = 400/d$ for the calculation of the dynamics under shear. At this value, the DCF

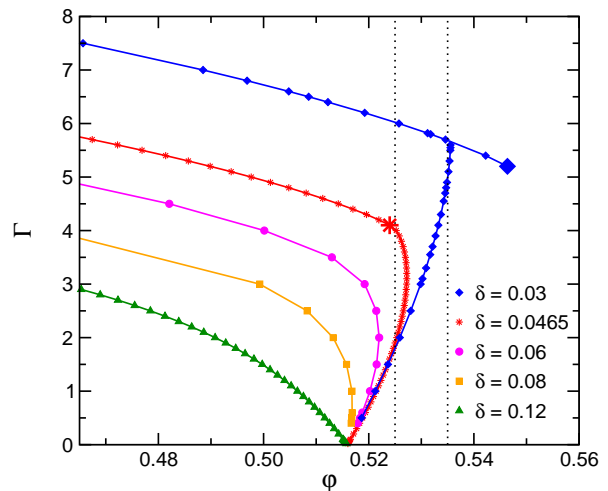


FIG. 1. Quiescent glass-transition diagram of the square-well system. Transition lines are shown in the packing-fraction–attraction-strength plane (φ, Γ) , for various attraction ranges δ as indicated. Dotted lines indicate paths considered in the following figures. For the $\delta = 0.0465$ and $\delta = 0.03$ curves, the bigger symbols mark approximate locations of the \mathcal{A}_4 and \mathcal{A}_3 higher-order singularities.

has decayed to zero to within less than 0.5% for all the state points considered below. An equidistant grid with step size $\Delta q = 0.2/d$ is chosen. Calculations for the quiescent glass-transition points have been obtained using $Qd = 240$ and $\Delta q d = 0.4$. The unit of length is fixed by the diameter of the hard spheres, $d = 1$, and $k_B T$ is the unit of energy. The Brownian unit of time for a colloidal system is then given by fixing the single-particle free diffusion coefficient, D_0 , as $\tau_0 = d^2/D_0 = 1$.

The quiescent static structure of the SWS model is evaluated in the mean-spherical approximation (MSA) and leading order of small well width δ . Here, an analytic expression for the DCF is readily available ([12]), allowing to efficiently calculate the MCT vertex.

III. RESULTS

Figure 1 shows the glass-transition diagram of the square-well system calculated from quiescent MCT ([12]). The $\Gamma = 0$ line reflects the pure hard-sphere system. Here, MCT predicts a glass transition at a critical packing fraction $\varphi_c \approx 0.516$. At large attraction range, $\delta > \delta^*$, this transition point extends into the φ – Γ -plane as a continuous line of glass transition points. According to MCT, these are bifurcations in the long-time behavior of the density correlation function, $f_q = \lim_{t \rightarrow \infty} \phi_q(t)$, where two solution branches of the nonlinear equations determining the nonergodicity factors f_q meet. They are termed \mathcal{A}_2 singularities in the mathematical classification of bifurcations.

Lowering δ below a critical value $\delta^* \approx 0.0465$, one recognizes at fixed attraction range two transition lines: a

repulsive- and an attractive-glass line cross at an intersection point. At this point, the repulsive-glass transition line (extending from the hard-sphere reference point) terminates, while the attractive-glass transition line continues as a glass-glass transition, terminating in an endpoint. Since all regular (repulsive and attractive) transition points are \mathcal{A}_2 singularities, this endpoint marks a higher-order singularity of type \mathcal{A}_3 . At $\delta = \delta^*$, this endpoint coincides with the crossing point, resulting in an even higher-order singularity, of type \mathcal{A}_4 . The occurrence of singularities of the \mathcal{A}_ℓ type is a topologically robust feature: changing the interaction potential somewhat, or modifying the approximations used in calculating the static structure functions, will not change the scenario qualitatively.

One also recognizes in Fig. 1 a reentry phenomenon when increasing the attraction strength Γ starting from the hard-sphere case, $\Gamma = 0$. For sufficiently short-ranged attractions, the repulsive-glass transition line first shifts to higher density, widening the region of the fluid and destabilizing the glass. Hence there exists a narrow density window, where the hard-sphere system is an ideal glass according to MCT, and first melts and then re-freezes as the attraction strength is increased. In agreement with the physical picture mentioned in the introduction ([15]), this only occurs if the attraction range exceeds the hard-core-caging length scale estimated by Lindemann, $\delta \gtrsim 0.1$. Intuitively, adding an attraction longer than Lindemann's localization length will not further bond particles at high density.

We begin by discussing typical flow curves upon crossing from the repulsive into the attractive glass. Figure 2 shows the case $\delta = 0.04$ at fixed density $\varphi = 0.525$, with increasing attraction strength Γ . At $\Gamma = 0$, the system is a repulsive glass, and exhibits a flowcurve of Herschel-Bulkley type: for $\dot{\gamma} \rightarrow 0$, a finite dynamic yield stress, $\sigma_y = \lim_{\dot{\gamma} \rightarrow 0} \sigma(\dot{\gamma}) > 0$, characterizes the flow-melted glass. The yield stress arises, because according to ITT-MCT, the nonlinear dynamic shear modulus $G(t)$ decays on the flow-induced time scale $\tau_{\dot{\gamma}} \sim 1/\dot{\gamma}$; in the glass, this is the only relevant time scale for long-time structural relaxation. In this regime, achieved for $\dot{\gamma} \rightarrow 0$, $G(t)$ becomes a function of $\dot{\gamma}t$ only, and the integral determining σ , Eq. (7), becomes independent on $\dot{\gamma}$ ([46]). The σ -versus- $\dot{\gamma}$ curve monotonically increases with increasing $\dot{\gamma}$. The limit of very high shear rates, $\dot{\gamma}\tau_0 \gg 1$, will not be discussed further in the following. It probes the interplay of flow and the short-time dynamics of the colloidal suspension, and MCT is not designed to treat this properly. The yield stress of the repulsive glass, σ_y^{rep} , is roughly given by $k_B T/d^3$, the entropic energy scale of the system.

As Γ is increased, the yield stress decreases slightly, indicating a weakening of the glass structure with weak attraction. Increasing Γ further, the reentrant glass transition is probed: as the quiescent glass state is molten by attraction, the flow curves show a Newtonian regime, $\sigma \propto \dot{\gamma}$, at low shear rates, indicative of a constant linear-

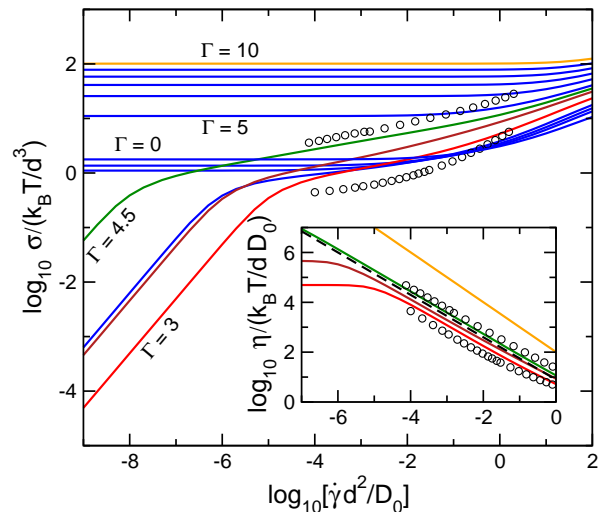


FIG. 2. Flowcurve $\sigma(\dot{\gamma})$ for the steady-state shear stress as a function of shear rate, for the square-well system with $\delta = 0.04$, at fixed packing fraction $\varphi = 0.525$, for increasing attraction strength (lines from bottom to top at high $\dot{\gamma}$: $\Gamma = 0, 1.0, 1.5, 2.0, 3.0, 4.0, 4.5, 5.0, 6.0, 7.0, 8.0, 9.0$, and 10.0). Inset: shear viscosity $\eta = \sigma/\dot{\gamma}$ corresponding to the $\Gamma = 3.0, 4.0, 4.5$, and 10.0 curves shown in the main figure. The dashed line indicates a power law $\propto \dot{\gamma}^{-0.85}$. Symbols are experimental data from Pham *et al.* [40], converted setting $k_B T/d^3 \equiv 3.5$ Pa and $\tau_0 = d^2/D_0 \equiv 0.002$ s.

response low-shear viscosity. The linear-response regime extends over small dressed Péclet numbers, $Pe = \dot{\gamma}\tau \ll 1$, where τ is the structural relaxation time of the fluid. For $Pe \gg 1$, a sublinear increase in $\sigma(\dot{\gamma})$ is reminiscent of the yield-stress plateau in the glass.

Further increasing Γ , the Newtonian low-shear viscosity first decreases, and then increases again, which is seen in the flow curves as first the lowering, and then the increase in the linear regime. Finally, the attractive glass is entered, and the flowcurves (in the ideal glass of ITT-MCT) display a true yield stress again. This yield stress of the attractive glass, σ_y^{attr} , is considerably higher than its repulsive counterpart. For the case shown in Fig. 2, it starts at approximately $10 k_B T/d^3$ for $\Gamma = 5$, and further increases to around $100 k_B T/d^3$ for $\Gamma = 10$. This strong increase is also responsible for the rise of the flow curves in the reentrant-fluid regime at intermediate $\dot{\gamma}$, where it leads to a crossing of the different σ -versus- $\dot{\gamma}$ curves for different Γ .

The yield stress increases by roughly a factor of ten when first crossing from the repulsive into the attractive glass. Although the numerical value will depend on the packing fraction, particle-size polydispersity and the details of the interaction potential, our result is in good agreement with the experimental data of Pham *et al.* [40]. Flowcurves measured by these authors, on a suspension of PMMA hard-sphere-like colloids with comparable attraction range, are shown in Fig. 2 as symbols. In this comparison, only two unknown scale factors are fixed:

shear rates $\dot{\gamma}$ given in absolute time units have to be converted to bare Péclet numbers $\dot{\gamma}\tau_0$ assuming a value for $\tau_0 = d^2/D_0$. From the Stokes-Einstein expression, one would obtain $\tau_0 \approx 0.01$ s for the system of Pham *et al.* [40]; however, taking into account the slowing down of free diffusion at high densities due to hydrodynamic interactions, we allow this value to be adjusted, setting $\tau_0 = 0.002$ s. The second parameter concerns the conversion of stresses into natural units. Given the approximations involved in our calculation for the simple SWS model, the agreement is reasonable. An even stronger increase in yield stress, by about a factor 100, has been found by Pandey and Conrad [7] upon increasing the attraction strength even further; this is again in quantitative agreement with our Fig. 2.

The inset of Fig. 2 displays the shear viscosities corresponding to selected flow curves shown in the main panel. The ideal-glass yield stress corresponds to shear-thinning behavior with a trivial shear-thinning exponent $x = 1$, i.e., $\eta \sim 1/\dot{\gamma}$. This regime is barely reached for the lowest shear rates in the experimental repulsive-glass data. The attractive-glass data do not show the approach to this asymptote within the experimentally accessible window. In the range covered there, an effective power law, $\eta \sim 1/\dot{\gamma}^x$ with $x < 1$ may be fitted to the data. This is apparent for the $\Gamma = 4.5$ curve in our ITT-MCT results, where $x \approx 0.85$ may reasonably be fitted to the η -versus- $\dot{\gamma}$ curve over more than four orders of magnitude of variation in shear rate. Such non-trivial shear-thinning exponents are routinely used to describe experimental data ([1, 48]), and have also been emphasized by Kobelev and Schweizer [45]. We stress that within ITT-MCT, they only appear as effective power laws describing the crossover from repulsive to attractive glass; both glass types are, within this theory, ultimately characterized by shear thinning with $x = 1$ at shear rates approaching zero.

The nonmonotonic variation in flow curves caused by the reentrant glass transition also translates to the viscosities. However, only the low- Pe regime of the curves reflects the quiescent ideal glass transition (defined as the point where the low-shear MCT viscosity diverges). Since the σ -versus- $\dot{\gamma}$ curves for different intermediate Γ cross, the viscosities probed at finite shear rates may exhibit a different ordering with respect to attraction strength.

The dependence of the yield stress on the attraction parameters is exemplified in Fig. 3 for those attraction strengths where the system remains glassy at the chosen fixed packing fraction. As anticipated from above, the repulsive-glass branch of $\sigma_y(\Gamma)$ decreases slightly with increasing Γ . The attractive-glass branch increases with increasing Γ . If one choses a path through the state diagram that crosses the glass-glass transition line, these two branches will cover the full Γ range, but still exhibit a finite jump at the Γ_c corresponding to the glass-glass transition. In the range of attraction ranges δ close to δ^* studied here, the yield stress is almost independent on δ along the attractive-glass branch. For strong attraction,

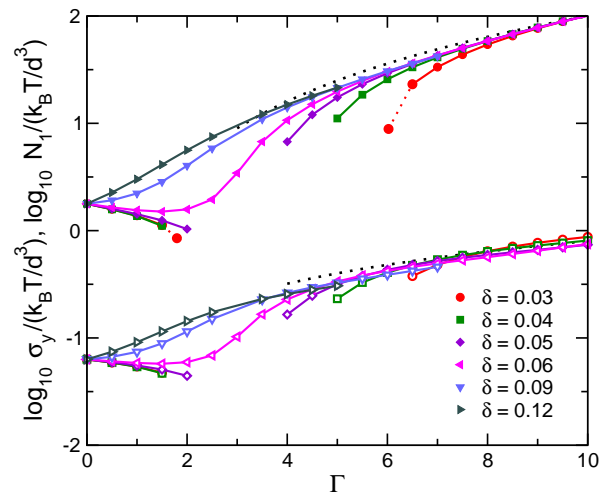


FIG. 3. Dynamic yield stress $\sigma_y = \lim_{\dot{\gamma} \rightarrow 0} \sigma(\dot{\gamma})$, as a function of attraction strength Γ at fixed packing fraction $\varphi = 0.525$, for various ranges δ as labeled (filled symbols). Data has been obtained setting $\dot{\gamma} = 10^{-9}$, showing only points where this shear rate is in the asymptotic regime. For the $\delta = 0.03$ curves, the points joined with dotted lines indicate the approach to the glass-transition points along the chosen path. Open symbols are the corresponding normal-stress differences N_1 . Dotted lines indicate the relations $\sigma_y \propto \Gamma^2$ (upper) and $N_1 \propto \Gamma$ (lower).

it can be described by $\sigma_y \sim \Gamma^y$ with some exponent y close to 2, and with a prefactor close to $k_B T / d^3$. For our data, $y \approx 2.2$ gives a good fit. Similar behavior has also been predicted by Kobelev and Schweizer [44] and seen in experiment, where different power laws have been observed and attributed to an oversimplification in the square-well model ([29]). A scaling with attraction strength with $y = 2$ is expected from the linear-response (Maxwell plateau) shear modulus G_∞ in this model: the attractive-glass line in MCT is dominated by contributions to the coupling vertex that scale as A^2/δ ([21]), where $A = \exp[\Gamma] - 1$. In the MSA structure factor employed in this work, the factor A arising from the Mayer cluster function is replaced by Γ . The weak dependence of σ_y on δ hints at the fact that the crossover from the linear-response regime to yielding depends linearly on the attraction range; this will be discussed below. This crossover also depends on the attraction strength to some extent, rationalizing why σ_y shows a somewhat stronger dependence on Γ as expected from G_∞ . For the larger δ , where the chosen line of constant packing fraction remains in the glass at all Γ , the repulsive- and attractive-glass branches of the σ_y -versus- Γ curves in Fig. 3 join smoothly. The case $\delta = 0.09$ is close to the point where the reentrant glass transition vanishes. Concomitantly, the yield stress in this case starts to increase monotonically with increasing Γ .

The yield-stress plateau in the flow curves becomes the more pronounced, the closer the system is to the respective glass transition. Thus, for states close to a

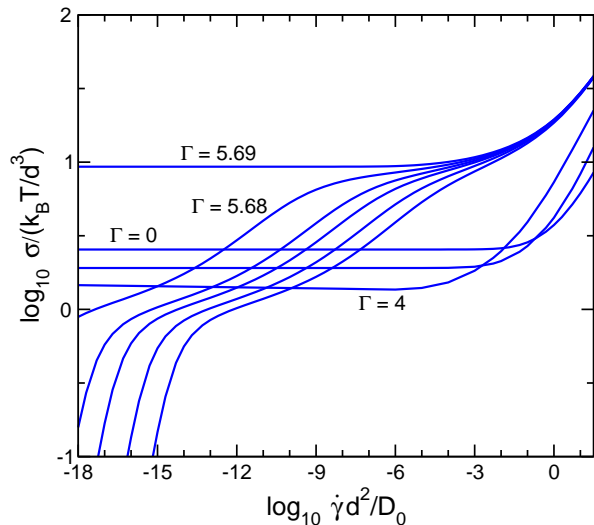


FIG. 4. Flowcurve $\sigma(\dot{\gamma})$ for the steady-state shear stress as a function of shear rate, for the square-well system with $\delta = 0.03$, at fixed packing fraction $\varphi = 0.535$, for increasing attraction strength (from bottom to top at large $\dot{\gamma}$: $\Gamma = 0, 2, 4, 5.61, 5.64, 5.66, 5.67, 5.68, \text{ and } 5.69$).

glass–glass transition, flowcurves with an indication of two plateaus, corresponding to σ_y^{rep} and σ_y^{attr} , can be expected. The flowcurves are monotonically increasing with increasing $\dot{\gamma}$, hence the repulsive-glass yield-stress plateau will appear at lower Pe , and the attractive-glass one at larger Pe . This is shown in Fig. 4 for the representative case $\delta = 0.03$ and $\varphi = 0.535$, for increasing attraction strength. In order to demonstrate the qualitative signature of the two glasses that emerges, a range of shear rates has to be shown that is unrealistically large for typical experiments or simulations.

As in Fig. 2, the hard-sphere reference case (dashed line in Fig. 4) exhibits a yield stress of the order $k_B T / d^3$. In Fig. 4 we do not focus on the weak-attraction regime since this is qualitatively the same as above. For the relatively strong attractions close to the glass–glass transition line, the repulsive-glass yield stress is already lowered appreciably, due to the softening of the glass connected to the reentrant fluidization. This is exhibited by the lower- Γ curves in Fig. 4: there, a repulsive-glass yield-stress plateau of $\mathcal{O}(k_B T / d^3)$ is visible around $Pe \approx 10^{-12}$, that is already well below the yield stress calculated for the hard-sphere system at this packing fraction. Since at $\varphi = 0.535$, these curves fall into the reentrant-fluidized region, they all display a linear Newtonian behavior at even lower Pe .

The curve for $\Gamma = 5.68$ in Fig. 4 demonstrates the approach to the glass–glass transition. The incipient arrest driven by attraction results in an additional, larger attractive-glass yield-stress plateau at higher (but still small) $Pe \approx 10^{-6}$. A flowcurve with two plateaus results. Within a window of shear rates that is realistically achievable in experiment or simulation, this distinction is

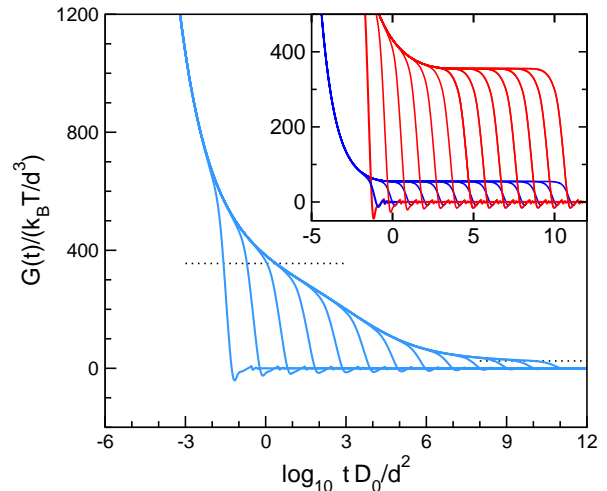


FIG. 5. Dynamical shear modulus $G(t)$ as a function of time t for the SWS with $\delta = 0.03$, packing fraction $\varphi = 0.535$, and attraction strength $\Gamma = 5.64$, close to the glass–glass transition. Various shear rates, $\dot{\gamma}\tau_0 = 10^n$ with $n = -12, -11, \dots, 0$, are shown. Dotted lines indicate the plateau moduli of the nearby attractive and repulsive glasses. The inset shows the corresponding plot for $\Gamma = 5.69$, inside the attractive glass (upper set of curves), and for the repulsive glass, $\Gamma = 0$ (lower set of curves).

not clearly visible. Rather, a broad window of sublinear rise in shear stress σ as a function of shear rate $\dot{\gamma}$ is characteristic for states close to the glass–glass transition, as was already discussed in connection with Fig. 2.

The behavior discussed above for the flowcurves reflects the non-trivial decay of the ITT-MCT correlation functions close to the glass–glass transition. Since the attractive glass is characterized by a larger nonergodicity parameter f_q than the repulsive glass, the quiescent density correlation functions are asymptotically governed by two plateaus: at short times, they relax to the larger f_q^{attr} , where they arrest in the attractive glass for sufficiently large Γ . For smaller Γ , they decay from this plateau towards the lower f_q^{rep} . For state points in the liquid, there then is a final relaxation from this plateau to zero. The intricacies of this three-step relaxation (as opposed to the common two-step relaxation in the vicinity of ordinary glass transitions) will not be discussed here in detail; we refer to the literature ([12, 58, 59]).

The asymptotic reasoning carries over to the dynamical shear modulus $G(t)$, Eq. (6). Essentially, one can distinguish three different scenarios for the decay of $G(t)$, depending on the ratio of the shear rate to the two relaxation times involved in the decay first from the attractive-glass plateau, τ^{attr} , and second from the repulsive-glass plateau, $\tau^{\text{rep}} \gg \tau^{\text{attr}}$. One can then introduce two different dressed Péclet numbers, $Pe^{\text{rep}} = \dot{\gamma}\tau^{\text{rep}}$ and $Pe^{\text{attr}} = \dot{\gamma}\tau^{\text{attr}}$. For $Pe^{\text{attr}} \ll Pe^{\text{rep}} \ll 1$, one recovers the quiescent equilibrium curve for $G(t)$, and hence linear response with a Newtonian shear viscosity. Increasing the shear rate, one enters a regime $Pe^{\text{rep}} \gg 1$

but $Pe^{\text{attr}} \ll 1$, where the stress is asymptotically given by the yield stress of the repulsive glass. Finally, in the regime $Pe^{\text{rep}} \gg Pe^{\text{attr}} \gg 1$, the stress is given by the yield stress of the attractive glass, until short-time relaxation effects become dominant at the highest shear rates. Since separating the two plateau regions in the correlation functions requires to fine-tune the parameters to the (liquid-side of the) crossing point of the two glass-transition lines in Fig. 1, the asymptotic behavior described above is unlikely to be clearly observed. This is seen in Fig. 5, where we plot in the main panel the dynamical shear modulus for the attraction strength $\Gamma = 5.64$ also considered in Fig. 4, and various shear rates, exemplifying the case close to the crossing of glass-transition lines. For $\dot{\gamma} \rightarrow 0$ these curves approach the quiescent correlation function that exhibits indications of a three-step relaxation process involving two plateaus, and a relaxation time $\tau^{\text{attr}} \sim 10^3 D_0/d^2$. Although this relaxation time is already very large, there still is no clearly recognizable attractive-glass plateau in $G(t)$. This is predicted by MCT for state points in the vicinity of higher-order transition points (such as the endpoint of the glass-glass transition line). There, the asymptotic description of two-step relaxation with a power law towards the plateau and a power-law decay from this plateau, is replaced by logarithmic decay laws ([13]), visible in semi-log plots such as Fig. 5 as straight lines. As shown in the inset of the figure, the dynamical shear moduli for the repulsive glass at $\Gamma = 0$, and the attractive glass at $\Gamma = 5.69$, clearly show the emergence of the related plateaus as the shear rate is lowered.

Shear induces a decay in $G(t)$ on a time scale $\tau_{\dot{\gamma}}$ that is for all states determined by the shear-flow time scale $1/\dot{\gamma}$. This decay fully decorrelates the fluctuations in ITT-MCT, so that no trace of the lower repulsive-glass plateau in $G(t)$ remains for large shear rates.

The $G(t)$ curves for large Péclet numbers show negative dips at late times in the relaxation. This has been discussed extensively in repulsive glasses ([41, 43, 50]). Since the time integral over $G(t)$ determines the shear stress, this corresponds to a nonmonotonic approach to the steady-state value σ and reflects the existence of a stress overshoot in the stress-strain curves measured after startup of steady flow. Since $G(t)$ is the autocorrelation function of microscopic stresses, this dip reflects an “elastic recoil” of breaking cages ([42, 60]).

The scaling of $\tau_{\dot{\gamma}}$ with $1/\dot{\gamma}$ as the only relaxation time that remains in the flow-melted ideal glass, implies that a master curve for the relaxation is obtained by scaling $G(t)$ by the plateau value G_{∞} and time by $\dot{\gamma}$. Figure 6 shows master curves obtained from the $\dot{\gamma} = 10^{-12}$ curves for the repulsive glass and the attractive glass at $\varphi = 0.535$ and $\delta = 0.03$. While the asymptotic laws of ITT-MCT describe generic behavior of the correlation functions around their plateau value, the details of the decay from this plateau to zero depend on the details of the interaction potential and state points. As exhibited in Fig. 6, the repulsive glass features a steeper decay to

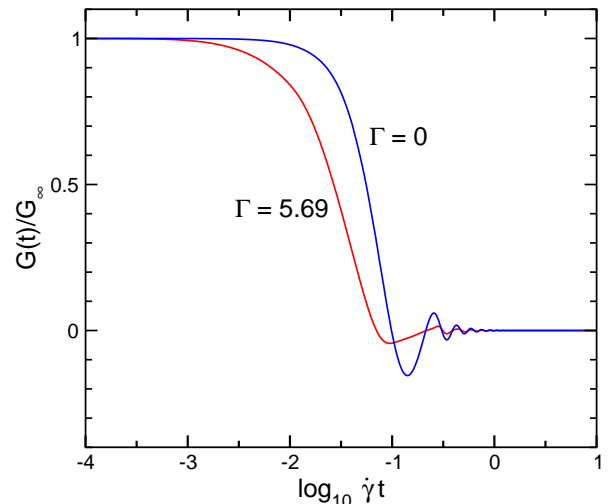


FIG. 6. Yield-stress master curves for the dynamical shear modulus of the SWS at $\delta = 0.03$ and $\varphi = 0.535$, for $\Gamma = 0$ (repulsive glass), and $\Gamma = 5.69$ (attractive glass), normalized by the plateau modulus G_{∞} , as a function of scaled time $\dot{\gamma}t$.

zero than the attractive-glass master curve for the value of Γ shown. Additionally, the coefficient relating $\tau_{\dot{\gamma}}$ to $1/\dot{\gamma}$ decreases with increasing attraction strength. In the repulsive glass, we obtain $\tau_{\dot{\gamma}} \approx \gamma_c/\dot{\gamma}$, in agreement with previous results ([41, 50]). Recall that the stress-strain curves are given by $\sigma_{xy}(\gamma) = \dot{\gamma} \int_0^t G(t) dt$ for $\gamma = \dot{\gamma}t$. This implies that the overshoot in the stress-strain curves of the repulsive glass occurs at a strain of roughly γ_c and corroborates our choice of $\gamma_c = 0.1$ to reflect the Lindemann criterion. In the attractive glass, the decay in $G(t)$ sets in earlier. This implies that the position of the overshoot in the stress-strain curves moves to lower strains with increasing Γ , as will be discussed in detail below.

We investigate the stress overshoots in more detail in Fig. 7. There, stress-strain curves $\sigma(\gamma)$ after startup of steady shear with various shear rates $\dot{\gamma}$ are shown for three representative cases: the repulsive glass, the attractive glass, and a state point close to the glass-glass transition. All curves show similar stress overshoots, showing that this feature is a robust signature of cage breaking, be it induced by the breaking of nearest-neighbor topology, or the breaking of individual bonds. The stress-strain curves for low Pe all show a linear elastic regime at small strains that is governed by the plateau value of the shear modulus, G_{∞} . The corresponding values obtained from the cases $\Gamma = 0$ and $\Gamma = 5.69$ are indicated in the figures as dash-dotted and dotted lines (cf. Fig. 5). At large Pe , shear-induced decay starts to set in already during the decay of $G(t)$ towards G_{∞} , and the elastic regime in $\sigma(\gamma)$ starts to correspond to the much higher short-time modulus G_0 . (The latter is formally infinite for true hard spheres.) This regime will not be discussed here. For the intermediate case close to the glass-glass transition, still lower shear rates would be required to probe the repulsive-glass linear-response G_{∞} .

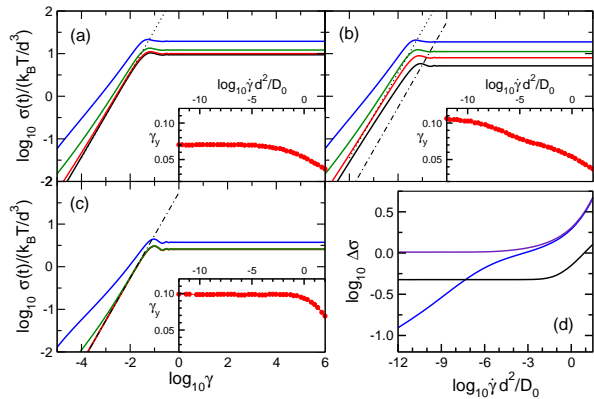


FIG. 7. Stress–strain curves after startup of steady shear, $\sigma(\gamma)$ for the cases shown in Fig. 5 and various shear rates $\dot{\gamma}\tau_0 = 10^n$ with $n = -6, -4, -2$, and 0 (bottom to top): (a) for the attractive-glass case, $\Gamma = 5.69$, (b) close to the glass–glass transition, $\Gamma = 5.64$, and (c) for the repulsive hard-sphere glass, $\Gamma = 0$. Dotted (dash-dotted) lines mark the linear-elastic plateau moduli G_∞ for the attractive (repulsive) glass cases. Insets show the dependence of the overshoot position γ_y as a function of shear rate. (d) Overshoot strength $\Delta\sigma = (\sigma_{\max} - \sigma) / \sigma_{\max}$ as a function of shear rate, for various Γ .

It should be noted that none of our stress–strain curves indicate the rich behavior at very large strain, $\gamma \approx 1$, that was seen in experiment ([28, 30, 39, 40]). Instead of a double-yielding scenario, ITT-MCT predicts both the repulsive and the attractive glass to yield at strains small compared to unity. In principle, the three-step decay of $G(t)$ induces several shoulders in the low- γ part of the stress–strain curve, but this concerns strains that are far below the experimental resolution, only probed at extremely small startup shear rates.

The mechanisms captured by ITT-MCT are more clearly borne out in the corresponding yield strain, i.e., the position of the maximum, $\sigma(\gamma_y) = \sigma_{\max}$. The dependence of γ_y on shear rate is shown in the insets of the first three panels in Fig. 7. The strong dependence that sets in at the highest shear rates shown are indicative of the cross-over to large bare Péclet numbers, and cannot be discussed correctly within the present ITT-MCT. Considering low shear rates for the repulsive glass, the stress overshoot occurs at a roughly rate-independent strain of $\gamma_y^{\text{rep}} \approx 0.1$, recovering the Lindemann criterion as discussed above. Since this value is essentially set by the model parameter γ_c in the isotropic approximation to ITT-MCT, it is not predictive.

In the attractive glass, we find $\gamma_y^{\text{rep}} \approx 0.07$ for the state point chosen here, again weakly dependent on shear rate for low enough Pe . This reproduces an effect discussed previously in experiment ([30]): the (first) yield strain of the attractive glass is lower than that of the repulsive glass. In the vicinity of the glass–glass transition, as explained above, the shear rate controls whether yielding is dominated by the attractive- or by the repulsive-glass

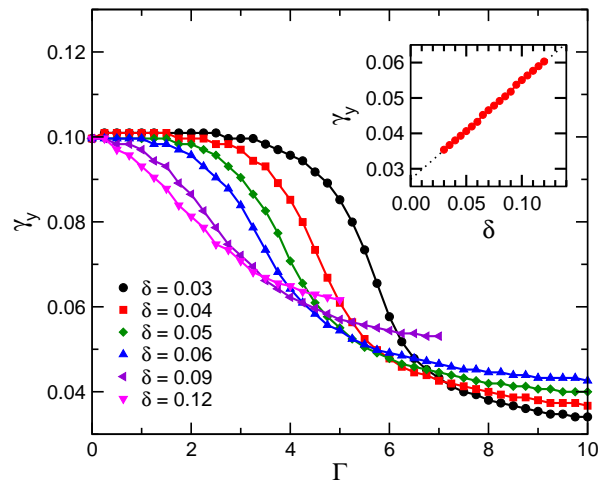


FIG. 8. Dependence of the yield strain γ_y on the attraction strength Γ for various attraction ranges δ as labeled, for strong shear, $Pe = 0.1$. The inset shows the dependence of the large- Γ asymptote on δ . A dotted line indicates a linear relation.

shear modulus. Indeed, for the $\Gamma = 5.64$ curves in Fig. 7, we observe a more pronounced dependence of γ_y on $\dot{\gamma}$. Its value decreases from $\gamma_y \approx \gamma_y^{\text{rep}}$ at the lowest shear rates to $\gamma_y \approx \gamma_y^{\text{attr}}$ at higher shear rates. This agrees with the discussion of $G(t)$ above.

The relative strength of the overshoot as compared to the steady-state value, $\Delta\sigma = (\sigma_{\max} - \sigma) / \sigma_{\max}$, is shown in the lower right panel of Fig. 7. For the repulsive and the attractive-glass limits, $\Delta\sigma$ is essentially independent on $\dot{\gamma}$ in the range of shear rates that are of interest here. This reflects the fact that within ITT-MCT, $G(t)$ approaches a master curve that depends only on $\dot{\gamma}t$ for states in the glass and in the limit $\dot{\gamma} \rightarrow 0$, as discussed in connection with Fig. 6. For the ultimately liquid state $\Gamma = 5.64$ shown in Fig. 7, the overshoot has to vanish as $\dot{\gamma} \rightarrow 0$, since in the linear-response regime $G(t)$ has to decay as a monotonically decreasing positive function ([60]). In effect, the $\Delta\sigma$ -versus- $\dot{\gamma}$ curves qualitatively resemble the corresponding flow curves.

Let us discuss in more detail the dependence of the (first) yield strain γ_y on the parameters of the square-well attraction. Figure 8 shows $\gamma_y(\Gamma)$ for various δ . The trend indicated already above becomes clear here: for each attraction range δ , there is a crossover from a repulsive-glass-like yielding at $\gamma_y^{\text{rep}} \approx 0.1$ at low attraction strength Γ , to a strong-attraction asymptote where $\gamma_y^{\text{attr}} < 0.1$. The value of Γ where this crossover occurs, increases with decreasing δ . For low δ , this can be rationalized by a concomitant trend in the glass–glass transition line which also moves to stronger attraction with decreasing square-well width.

The large- Γ asymptote obeys $\gamma_y^{\text{attr}} \propto \delta$ with some offset, as shown in the inset of Fig. 8. This is in line with the reasoning that the yield strain in the attractive glass is eventually set by the length of a bond. It should however be noted that the constant of proportionality is less

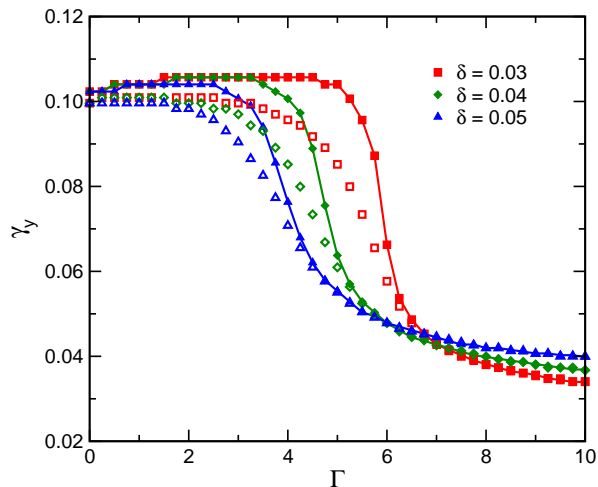


FIG. 9. As in Fig. 8, but for a lower shear rate $Pe = 10^{-3}$ (filled symbols). Open symbols repeat the data of Fig. 8 ($Pe = 0.1$) as a reference.

than unity. Due to the offset, $\gamma_y^{\text{attr}}(\delta=0) > 0$ holds, but recall that the large- Γ asymptote in this limit would only be obtained for $\Gamma \rightarrow \infty$, i.e., Baxter's adhesive-sphere limit ([10, 12]). For small δ , we thus obtain $\gamma_y^{\text{attr}} \gtrsim \delta$ (cf. the case $\delta = 0.03$ in our calculations). But already for slightly larger attraction ranges, $\gamma_y^{\text{attr}} \lesssim \delta$. In particular, up to $\delta = 0.12$ we still find $\gamma_y^{\text{attr}} < \gamma_y^{\text{rep}}$ and $\gamma_y^{\text{attr}} \sim \delta$, while the argument based on the Lindemann length scale would suggest that at such large δ , the yielding of cages should come first. One should however recall that the Lindemann length is only a rough estimate, and that this cage-induced length scale will also decrease upon entering deeper into the glass. Let us also note in this context, that at large Γ , one approaches the spinodal of the SWS model, which may bring in additional physical mechanisms. We have restricted all data points to be sufficiently far from the spinodal to not be qualitatively influenced by it.

The two trends described above lead to a crossing of the γ_y -versus- Γ for different δ . This in turn implies that for weak attraction strength, there is a regime where γ_y decreases with increasing attraction range, or even shows nonmonotonic behavior with δ . In this regime, γ_y is not indicative of the breaking of bonds, but rather reflects the easier fluidization of the weakly attractive glass, as compared to the hard-sphere reference.

The position of γ_y depends weakly on the shear rate, and it does most noticeably so in the intermediate- Γ regime close to the glass-glass transition (cf. insets in Fig. 7). Hence, the γ_y -versus- Γ curves may display additional behavior in the crossover regime for different shear rates. This is exemplified in Fig. 9, where results corresponding to those shown in Fig. 8 are repeated for lower Pe . For large Γ , the overshoot position does not depend strongly on Pe . Hence, the curves for same δ agree in this limit. But for the $\delta \lesssim \delta^*$ curves displayed in the fig-

ure, a weak non-monotonic behavior in $\gamma_y(\Gamma)$ is observed at intermediate Γ : Up to $\Gamma \approx 3$, the yield strain for, say, $\delta = 0.03$ and $Pe = 10^{-3}$ first increases slightly with increasing Γ , before it decreases to the expected large- Γ asymptote. An increase of γ_y with increasing Γ has also been observed in full anisotropic ITT-MCT calculations ([51]). For the shear rate shown in Fig. 9, we only find nonmonotonic behavior in $\gamma_y(\Gamma)$ for small enough δ , but not for $\delta = 0.09$ or $\delta = 0.12$ (not shown).

The mechanism of shear-advected loss of contributions to the MCT coupling coefficients allows to qualitatively explain the initial increase in γ_y with increasing Γ : adding weak attractions to the hard-sphere system, the first effect observed in the static structure factor S_q (and thus similarly in the DCF c_q) is a lowering of the peak amplitudes, combined with an increase in peak widths ([12]). The lowering of amplitude is responsible for the attraction-induced weakening of the glass. Yielding within ITT-MCT occurs at the point where the accumulated strain is sufficient to decorrelate the advected and non-advected contributions to $V_{\vec{q}, \vec{k}}^{(\dot{\gamma})}$, cf. Eq. (3). For those regions where the broadening of the peaks in c_q is still dominant over its overall loss of amplitude, the decorrelation will require larger strains than in the hard-sphere reference state. Hence, $\gamma_y(\Gamma)$ initially increases, as shown in Fig. 9. For stronger attractions, the growing large- q tail of c_q becomes more dominant. The attraction range δ in this case governs the large- q periodicity of the DCF, so that decorrelation in Eq. (3) is achieved by strains that themselves scale with δ .

The finding that $\gamma_y \sim \delta$ independent on Γ in the strong-attraction limit, provides a qualitative explanation for the independence of the yield stress on δ that was discussed in connection with Fig. 3. Noting that the shear-induced decay in $G(t)$ is exponential or faster, the integral determining the yield stress is dominated by the area under the plateau of height G_∞ , cut off at the time where $\dot{\gamma}t \approx \gamma_y$. As a result, $\sigma_y \sim G_\infty \gamma_y$. Recalling the above-mentioned scaling of G_∞ , one gets $\sigma_y \sim (\Gamma^2/\delta) \cdot \delta$, which is independent on δ .

The dependence of the maximum stress at the yield strain, $\sigma_{\text{max}} = \sigma(\gamma_y)$, on the attraction strength Γ is documented in Fig. 10. At the largest Γ shown, σ_{max} depends only weakly on the range δ , and increases strongly with Γ . This is in qualitative agreement with the behavior predicted for the dynamic yield stress discussed above. For σ_{max} , the increase with Γ is found to be slightly stronger than Γ^2 , and can be fitted with an effective power law, Γ^α with $\alpha \approx 2.2$, in the range shown in Fig. 10. This is similar to the behavior found for the steady-state dynamic yield stress, cf. Fig. 3. As already found for γ_y , the crossover into this strong-attraction regime scales with the position of the glass-glass transition and hence shifts to larger Γ with decreasing δ . This is demonstrated in the inset of Fig. 10, where σ_{max} is shown versus the square-well attraction area $\Gamma \cdot \delta$.

At intermediate Γ , a minimum in the σ_{max} -versus- Γ curve is seen. This is again a signature of the reen-

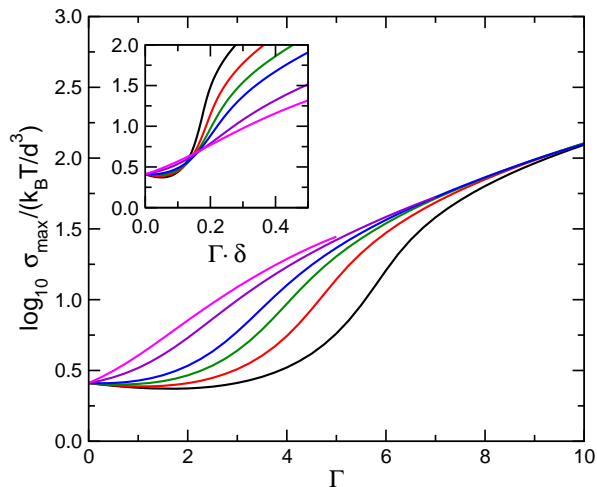


FIG. 10. Dependence of the maximum stress σ_{\max} at yielding on the attraction strength Γ in the square-well system, for packing fraction $\varphi = 0.525$ and $\dot{\gamma} = 0.1$. Various attraction ranges $\delta = 0.03, 0.04, 0.05, 0.06, 0.09,$ and 0.12 , are shown (increasing from bottom to top). The inset shows the same data versus the attraction area $\Gamma \cdot \delta$.

trant glass melting. The initial decrease with increasing Γ reflects the weakening of the glass due to weak attraction: it agrees with the decrease of the yield stress shown in Fig. 3 and the observation that the relative stress-overshoot height is insensitive to the attraction parameters. Note that in Fig. 10, a finite Péclet number, $Pe = 0.1$, was chosen. Hence, an overshoot is still observed in the attraction-melted fluid at intermediate Γ , where in Fig. 3 no true yield stress could be defined.

We now turn to a brief discussion of the relation between shear viscosity and the first normal-stress coefficient. Farage *et al.* [57] have investigated this relationship using the full, anisotropic ITT-MCT, in an expansion of small shear rates. Following this work, we present in Fig. 11 the results for the shear viscosity η and the first normal-stress coefficient Ψ_1 as functions of packing fraction φ from the isotropic model for a constant- Γ path through configuration space. Qualitatively, our results agree very well with those of Farage *et al.* [57], cf. their Fig. 2, although one has to keep in mind that these authors were discussing a hard-core Yukawa potential as a model for a short-ranged attractive colloid, instead of the SWS. This difference notwithstanding, we confirm that the isotropic ITT-MCT model produces very similar results to the anisotropic theory in this limit. As the packing fraction is increased, both the viscosity and the normal-stress coefficient increase strongly since the glass transition is approached. This increase sets in at lower packing fractions for stronger attractions, as expected from the glass-transition diagram, Fig. 1. Ψ_1 is about one order of magnitude smaller than η at low densities, but diverges more quickly towards the transition. This is in quantitative agreement with the low- $\dot{\gamma}$ limit of the full theory ([57]). There, also the second normal-stress coefficient

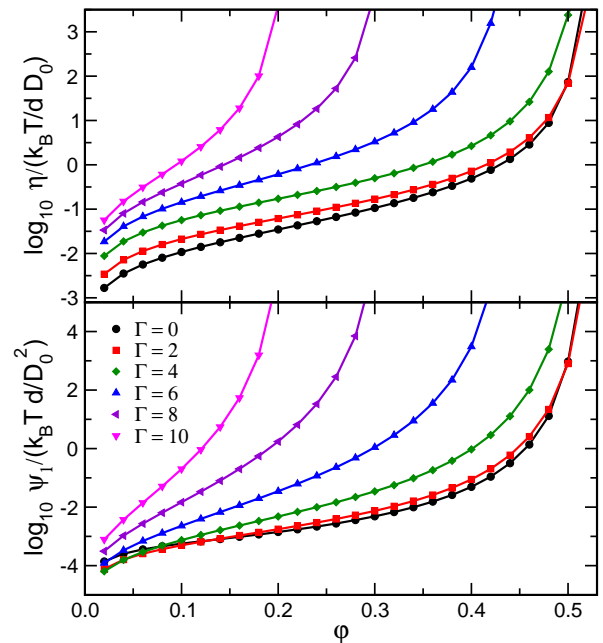


FIG. 11. Low-shear viscosity $\eta = \sigma/\dot{\gamma}$ (upper panel) and first normal-stress coefficient $\Psi_1 = (\sigma_{xx} - \sigma_{yy})/\dot{\gamma}^2$ (lower panel) as functions of packing fraction φ , for various attraction strengths of the SWS model with $\delta = 0.05$, and for shear rate $\dot{\gamma}\tau_0 = 10^{-4}$.

coefficient Ψ_2 was investigated. It remains approximately one order of magnitude below Ψ_1 throughout. Our isotropic approximation, which entails setting $\Psi_2 = 0$, hence seems justified in this respect.

To investigate the relevant wave-number range contributing to the ITT-MCT integrals for the shear stress and the first normal-stress coefficient, we discuss the corresponding integrand functions $I_\eta(k)$ and $I_{\Psi_1}(k)$. For this discussion, we consider low volume fractions, to make contact with the work of Farage *et al.* [57]. Our results from the isotropic ITT-MCT are shown in Fig. 12. First one recognizes strong oscillations in the integrands, anti-phased to the oscillations of the static structure factor: the latter, e.g., has a peak at $k = k_{\max} \approx 2\pi/d$, while both I_η and I_{Ψ_1} display a minimum there. This is clear since the mode-coupling vertices entering the Green-Kubo relation, Eq. (6), contain derivatives of S_k .

As the density is increased, the integrand increases at all k , but more strongly at k below and above the position of the first diffraction peak, k_{\max} . This reflects the increase in nearest-neighbor caging. At the same time, I_{Ψ_1} decays more rapidly at large k than I_η . This is particularly clear in a double-logarithmic representation of these functions, as shown in the insets of Fig. 12. There one recognizes power-law asymptotes followed by the maxima. In I_η , there is an intermediate regime where $|I_\eta(k)| \sim 1/k$ for $1/d \ll k \ll 1/\delta$ (dashed lines in the inset). For $k \gg 1/\delta$, $|I_\eta(k)| \sim 1/k^2$ is observed, modulated by oscillations whose periodicity is set by the smaller length scale δ . This crossover from slow $1/k$ decay to

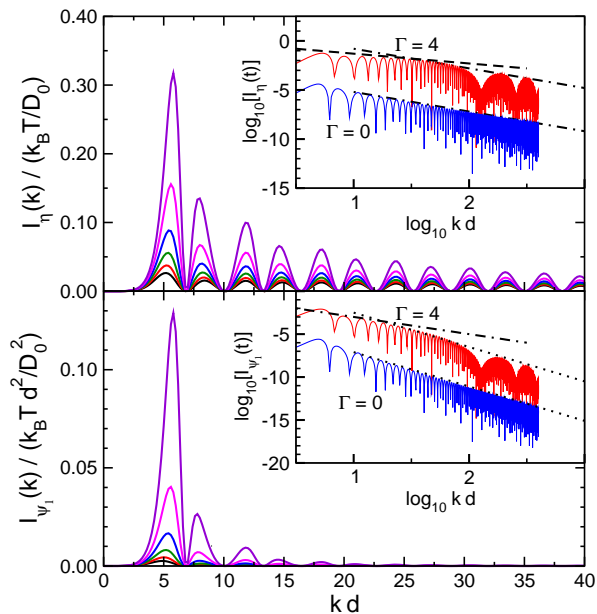


FIG. 12. Viscosity- and normal-stress-coefficient integrands $I_\eta(k)$ (upper panel) and $I_{\Psi_1}(k)$ (lower panel), as a function of wave number k in the isotropic ITT-MCT model. Different curves correspond to increasing packing fraction (increasing from bottom to top: $\varphi = 0.16, 0.20, 0.24, 0.28, 0.32$, and 0.36), for $\Gamma = 4$, $\delta = 0.05$, and $\dot{\gamma}\tau_0 = 10^{-4}$. The insets show the $\varphi = 0.24$ results in a double-logarithmic representation. Dashed lines indicate $1/k$ laws, dash-dotted lines $1/k^2$, and dotted lines $1/k^4$ laws for comparison. Here, results for the purely repulsive case, $\Gamma = 0$, have also been added, shifted down by a factor 1000 for clarity.

a faster $1/k^2$ decay reflects the same crossover occurring in the DCF, and discussed in detail for the physics of the quiescent SWS-MCT ([12]). With decreasing attraction range, the slow $1/k$ decay extends further out in reciprocal space, indicating that for very short-ranged attractive glasses, features in the mode-coupling vertex at large k remain important, while close to the repulsive glass, the k range around k_{\max} is the dominant one. This has also been found in computer simulation ([61]). This is of course simply the observation that the Fourier transform reflects the discontinuities of the SWS potential.

Interestingly, the normal stresses are less dominated by large k . This is evident from Fig. 12, where the corresponding envelopes for $|I_{\Psi_1}|$ are found to closely match $\sim 1/k^2$ and $\sim 1/k^4$, respectively. The same effect is present in the work of Farage *et al.* [57], although there it was not commented upon. A simple argument allows to qualitatively understand the faster decay for the normal-stress integrand, starting from the wave-vector dependent integrands defining $I_\eta(k)$, Eq. (9), and $I_{\Psi_1}(k)$, Eq. (10). These time integrals contain a long-time cutoff due to the shear-induced decay of the density correlation function, on a time scale $\sim 1/\dot{\gamma}$, modulated by k -dependent prefactors arising from the advected structure functions. Suppose this can be captured by a k -dependent effec-

tive cutoff time scale $\tau(k)/\dot{\gamma}$. Then, up to trivial prefactors, $\dot{\gamma}I_\eta(k) \approx \dot{\gamma} \int_0^\infty dt \exp[-\dot{\gamma}t/\tau(k)] = \tau(k)$, while $\dot{\gamma}^2 I_{\Psi_1}(k) \approx \dot{\gamma}^2 \int_0^\infty dt t \exp[-\dot{\gamma}t/\tau(k)] = \tau(k)^2$. Hence, the envelopes determining the large- k decay of $I_\eta(k)$, $1/k$ and $1/k^2$, translate approximately into $1/k^2$ and $1/k^4$ for $I_{\Psi_1}(k)$. As a result, the dependence of the normal-stress difference N_1 on the attraction strength is weaker than that of the shear stress σ . This is exemplified by Fig. 3. There, N_1 displays a weaker increase with Γ in the attractive-glass regime; it is well described by $N_1 \propto \Gamma$, as compared to the stronger $\sigma_y \propto \Gamma^2$.

We also note that in Farage *et al.* [57], a very prominent low- k structure was seen in $I_\eta(k)$ (but less so in $I_{\Psi_1}(k)$). Such a strong peak at $k \ll 2\pi/d$ is not present in our results. This reflects the different treatment of wave-vector advection between the isotropic and the anisotropic ITT-MCT, resulting also in a different definition of the integrand functions that are discussed. It may also be due to the fact that in Farage *et al.* [57] states closer to the liquid-gas spinodal were considered.

IV. DISCUSSION

The ITT-MCT model predicts the yield stress to increase by roughly a factor of ten upon crossing over from the repulsive glass to the attractive glass, for packing fractions close to the repulsive-glass transition, and for size ratios close to the one where glass-glass transitions first emerge. The precise value will depend on the interaction details, size polydispersity, and the packing fraction, but qualitatively, experimental data by Pham *et al.* [40] agree with this result, as shown in Fig. 2. Regarding these data, the authors noted that in the attractive glass, no clear yield-stress plateau was observed even for the lowest $\dot{\gamma}$ reached in the experiment. As shown in Fig. 2, this may be because the attractive glass is not quite reached, and an intermediate sublinear crossover from the higher attractive-glass stress probed at high Pe , to the repulsive-glass stress probed at low Pe covers a broad window of shear rates. However, one also has to keep in mind, that the attractive glass as predicted by MCT is a theoretical idealization. Activated processes, more dominant than in the repulsive-glass regime ([16]), as well as aging effects that are excluded from our theoretical description may be responsible for the disappearance of a clear attractive-glass yield-stress plateau.

In the vicinity of glass-glass transitions, the nonlinear rheology of short-range attractive systems should in principle reflect the intricate multi-step relaxation patterns of the quiescent dynamics. Close to the higher-order singularities of MCT, one indeed expects flow curves that have logarithmic corrections, due to the logarithmic asymptotic laws for the MCT correlation functions close to these points. However, the distinction between attractive and repulsive glass is only an asymptotic one at intermediate attraction strength; mapping the approach to this asymptote will require to cover unfeasibly large win-

dows in shear rate, and to fine-tune model parameters. In typical experiments, the physics of the glass–glass transition will hence rather manifest itself in preasymptotic features, such as the effective non-trivial shear-thinning power laws discussed in Fig. 2.

The ITT-MCT yield stress of the repulsive glass is given by the entropic energy-density scale, $\sigma_y^{\text{rep}} \sim k_B T/d^3$. In the attractive glass, the attraction strength Γ takes over the role of the energy scale, leading to $\sigma_y^{\text{attr}} \sim k_B T \Gamma^2/d^3 \sim U_0(U_0/k_B T)$. This dependence on the attraction strength reflects that of the linear-response shear moduli. It provides an interesting perspective on recent discussions of low-temperature glass rheology and the crossover from entropic glass transitions to “athermal” ones driven by interparticle interaction energies ([62]). Our calculations demonstrate how non-entropic yield stresses may emerge from ITT-MCT.

Since σ_y^{attr} is insensitive to the attraction range, this indicates that the ITT-MCT yielding criterion is one of strain-induced energy: the energy at which the glass yields is related to the energy of the interparticle attraction, i.e., a certain number of bonds that are broken by the deformation, and less crucially the amount of strain needed to break such bonds.

Our isotropic-ITT-MCT calculations do not capture the two-step yielding that was emphasized in experiments of Pham *et al.* [39, 40], and later confirmed ([28, 30, 63]). The delicate balance between attraction- and repulsion-dominated contributions to the dynamical shear modulus concerns, in the case where both of them are seen, very small strains that are not resolved in experiment. Within ITT-MCT, strains of $\gamma \approx 1$ are already well into the stationary regime, while in the mentioned experiments, this was the position of the second yielding point. It is unlikely that the full angle-resolved ITT-MCT will recover the two-step yielding, and first numerical results confirm this ([51]). Apart from appealing to the known aging- and hopping-induced relaxation phenomena that become relevant in the attractive glass, a possible resolution of this discrepancy may lie in the fact that the second yielding can be attributed to the breaking up of larger clusters of particles, reminiscent of the heterogeneous nature of the attractive glass. Such aspects are not captured in the present ITT-MCT.

This issue notwithstanding, one may identify the yield strain obtained by ITT-MCT with the first yielding point observed in experiment. The predictions of the theory regarding its dependence on attraction strength and range can then in principle be tested.

V. CONCLUSIONS

We have discussed aspects of the steady-state nonlinear rheology and yielding of dense colloidal suspensions of hard-core particles with a short-ranged attraction, within ITT-MCT and an isotropic approximation to its correlation functions. Our emphasis was on the transition from repulsive to attractive glasses and the manifestation of attraction-induced reentrant melting and glass–glass transitions in nonlinear rheology. The dynamic yield stress, defined as the $\dot{\gamma} \rightarrow 0$ limit of the steady-state flow curves, was found to increase strongly with the attraction strength, while it is largely independent on the attraction range. Similar conclusions hold for the maximum stress observed in the stress–strain curves measured in startup flow; a quantity that is often also referred to as a yield stress. The corresponding yield strain scales with the attraction range at strong attractions, and reflects the interplay of weakening and stabilizing of the glass at low attraction strengths. The first normal-stress difference was found to be less sensitive to attraction than the shear stress.

While the phenomena of double-yielding in startup flow that were reported in experiment are not explained by the current theory, this failure may be connected to additional cluster formation at very strong attractions. It will be interesting to see whether the ITT-MCT predictions can be found for systems with weak attraction strengths.

In applying ITT-MCT to attractive glasses one should recall that the theory, at present, presupposes the existence of a homogeneous flow field. This issue also arises in repulsive glasses, where shear banding occurs in certain parameter regimes ([64]). Attractive systems, however, may be more susceptible to shear banding ([65]).

It will be intriguing to see whether a combination of ITT-MCT with the cluster-MCT proposed by Kroy *et al.* [23] can explain the second yield step reported for attractive glasses. The cluster-MCT approach combines (quiescent) MCT with the notion of an RG-like flow in parameter space, in order to account for the slow aggregation of particles.

ACKNOWLEDGMENTS

We thank M. Fuchs for discussions. M. P. thanks for funding from DLR-DAAD fellowship No. 141. Th. V. thanks for funding from the Helmholtz Gemeinschaft (HGF VH-NG 406).

-
- [1] R. G. Larson, *The Structure and Rheology of Complex Fluids* (Oxford University Press, Oxford, UK, 1998).
 - [2] R. J. Farris, *Trans. Soc. Rheol.* **12**, 281 (1968).
 - [3] J. E. Funk and D. R. Dinger, *Predictive Process Con-*

- trol Of Crowded Particulate Suspensions: Applied To Ceramic Manufacturing* (Springer, New York, 1993).
- [4] C. Servais, R. Jones, and I. Roberts, *J. Food Eng.* **51**, 201 (2002).

- [5] A. T. J. M. Woutersen and C. G. de Kruif, *J. Chem. Phys.* **94**, 5739 (1991).
- [6] J. A. Lewis, *J. Am. Ceram. Soc.* **83**, 2341 (2000).
- [7] R. Pandey and J. C. Conrad, *Soft Matter* **8**, 10695 (2012).
- [8] N. Willenbacher, J. S. Vesaratchanon, O. Thorwarth, and E. Bartsch, *Soft Matter* **7**, 5777 (2011).
- [9] S. Asakura and F. Oosawa, *J. Chem. Phys.* **22**, 1255 (1954).
- [10] L. Fabbian, W. Götze, F. Sciortino, P. Tartaglia, and F. Thiery, *Phys. Rev. E* **59**, 1347(R); **60**, 2430 (E) (1999).
- [11] J. Bergenholtz and M. Fuchs, *Phys. Rev. E* **59**, 5706 (1999).
- [12] K. Dawson, G. Foffi, M. Fuchs, W. Götze, F. Sciortino, M. Sperl, P. Tartaglia, Th. Voigtmann, and E. Zaccarelli, *Phys. Rev. E* **63**, 011401 (2000).
- [13] W. Götze and M. Sperl, *Phys. Rev. E* **66**, 011405 (2002).
- [14] M. Sperl, *Phys. Rev. E* **68**, 031405 (2003).
- [15] F. Sciortino, *Nature Mater.* **1**, 145 (2002).
- [16] F. Sciortino, P. Tartaglia, and E. Zaccarelli, *Phys. Rev. Lett.* **91**, 268301 (2003).
- [17] T. Eckert and E. Bartsch, *Phys. Rev. Lett.* **89**, 125701 (2002).
- [18] K. N. Pham, A. M. Puertas, J. Bergenholtz, S. U. Egelhaaf, A. Moussaïd, P. N. Pusey, A. B. Schofield, M. E. Cates, M. Fuchs, and W. C. K. Poon, *Science* **296**, 104 (2002).
- [19] K. N. Pham, S. U. Egelhaaf, P. N. Pusey, and W. C. K. Poon, *Phys. Rev. E* **69**, 011503 (2004).
- [20] J. Bergenholtz and M. Fuchs, *J. Phys.: Condens. Matter* **11**, 10171 (1999).
- [21] J. Bergenholtz, M. Fuchs, and Th. Voigtmann, *J. Phys.: Condens. Matter* **12**, 6575 (2000).
- [22] S. A. Shah, Y.-L. Chen, K. S. Schweizer, and C. F. Zukoski, *J. Chem. Phys.* **119**, 8747 (2003).
- [23] K. Kroy, M. E. Cates, and W. C. K. Poon, *Phys. Rev. Lett.* **92**, 148302 (2004).
- [24] A. M. Puertas, M. Fuchs, and M. E. Cates, *Phys. Rev. Lett.* **88**, 098301 (2002).
- [25] A. M. Puertas, M. Fuchs, and M. E. Cates, *Phys. Rev. E* **67**, 031406 (2004).
- [26] A. M. Puertas, M. Fuchs, and M. E. Cates, *J. Chem. Phys.* **121**, 2813 (2004).
- [27] E. Zaccarelli and W. C. K. Poon, *Proc. Natl. Acad. Sci. (USA)* **106**, 15203 (2009).
- [28] M. Laurati, G. Petekidis, N. Koumakis, F. Cardinaux, A. B. Schofield, J. M. Brader, M. Fuchs, and S. U. Egelhaaf, *J. Chem. Phys.* **130**, 134907 (2009).
- [29] M. Laurati, S. U. Egelhaaf, and G. Petekidis, *J. Rheol.* **55**, 673 (2011).
- [30] N. Koumakis and G. Petekidis, *Soft Matter* **7**, 2456 (2011).
- [31] C. J. Rueb and C. F. Zukoski, *J. Rheol.* **42**, 1451 (1998).
- [32] V. Prasad, V. Trappe, A. D. Dinsmore, P. N. Segre, L. Cipelletti, and D. A. Weitz, *Faraday Discuss.* **123**, 1 (2003).
- [33] S. B. Lindström, T. E. Kodger, J. Sprakel, and D. A. Weitz, *Soft Matter* **8**, 3657 (2012).
- [34] J. Grandjean and A. Mourchid, *Europhys. Lett.* **65**, 712 (2004).
- [35] M. Sztucki, T. Narayanan, G. Belina, A. Moussaïd, F. Pignon, and H. Hoekstra, *Phys. Rev. E* **74**, 051504 (2006).
- [36] T. Narayanan, M. Sztucki, G. Belina, and F. Pignon, *Phys. Rev. Lett.* **96**, 258301 (2006).
- [37] C. Mayer, E. Stiakakis, E. Zaccarelli, C. N. Likos, F. Sciortino, P. Tartaglia, H. Löwen, and D. Vlassopoulos, *Rheol. Acta* **46**, 611 (2007).
- [38] D. Truzzolillo, D. Marzi, J. Marakis, B. Capone, M. Cargano, A. Munam, F. Moingeon, M. Gauthier, C. N. Likos, and D. Vlassopoulos, *Phys. Rev. Lett.* **111**, 208301 (2013).
- [39] K. N. Pham, G. Petekidis, D. Vlassopoulos, S. U. Egelhaaf, P. N. Pusey, and W. C. K. Poon, *Europhys. Lett.* **75**, 624 (2006).
- [40] K. N. Pham, G. Petekidis, D. Vlassopoulos, S. U. Egelhaaf, W. C. K. Poon, and P. N. Pusey, *J. Rheol.* **52**, 649 (2008).
- [41] J. Zausch, J. Horbach, M. Laurati, S. U. Egelhaaf, J. M. Brader, Th. Voigtmann, and M. Fuchs, *J. Phys.: Condens. Matter* **20**, 404210 (2008).
- [42] N. Koumakis, M. Laurati, S. U. Egelhaaf, J. F. Brady, and G. Petekidis, *Phys. Rev. Lett.* **108**, 098303 (2012).
- [43] C. P. Amann, F. Weysser, M. Fuchs, M. Siebenbürger, M. Krüger, and M. Ballauff, *J. Rheol.* **57**, 149 (2013).
- [44] V. Kobelev and K. S. Schweizer, *Phys. Rev. E* **71**, 021401 (2005).
- [45] V. Kobelev and K. S. Schweizer, *J. Chem. Phys.* **123**, 164903 (2005).
- [46] M. Fuchs and M. E. Cates, *Phys. Rev. Lett.* **89**, 248304 (2002).
- [47] M. Fuchs and M. E. Cates, *J. Rheol.* **53**, 957 (2009).
- [48] J. M. Brader, *J. Phys.: Condens. Matter* **22**, 363101 (2010).
- [49] O. Henrich, F. Weysser, M. E. Cates, and M. Fuchs, *Phil. Trans. Roy. Soc. A* **367**, 5033 (2009).
- [50] M. Fuchs and M. E. Cates, *Faraday Discuss.* **123**, 267 (2003).
- [51] C. P. Amann and M. Fuchs, (2013), this issue.
- [52] J. M. Brader, Th. Voigtmann, M. Fuchs, R. G. Larson, and M. E. Cates, *Proc. Natl. Acad. Sci. (USA)* **106**, 15186 (2009).
- [53] W. Götze, *Complex Dynamics of Glass-Forming Liquids* (Oxford University Press, Oxford, 2009).
- [54] J. M. Brader, Th. Voigtmann, M. E. Cates, and M. Fuchs, *Phys. Rev. Lett.* **98**, 058301 (2007).
- [55] J. M. Brader, M. E. Cates, and M. Fuchs, *Phys. Rev. Lett.* **101**, 138301 (2008).
- [56] J. Salençon, *Handbook of Continuum Mechanics* (Springer, New York, 2001).
- [57] T. F. F. Farage, J. Reinhardt, and J. M. Brader, *Phys. Rev. E* **88**, 042303 (2013).
- [58] M. Fuchs, W. Götze, I. Hofacker, and A. Latz, *J. Phys.: Condens. Matter* **3**, 5047 (1991).
- [59] M. Sperl, *Phys. Rev. E* **69**, 011401 (2004).
- [60] M. Siebenbürger, M. Ballauff, and Th. Voigtmann, *Phys. Rev. Lett.* **108**, 255701 (2012).
- [61] A. M. Puertas, E. Zaccarelli, and F. Sciortino, *J. Phys.: Condens. Matter* **17**, L271 (2005).
- [62] A. Ikeda and L. Berthier, *Phys. Rev. E* **88**, 052305 (2013).
- [63] N. Koumakis, A. Pamvouxoglou, A. S. Poulos, and G. Petekidis, *Soft Matter* **8**, 4271 (2012).
- [64] R. Besseling, L. Isa, P. Ballesta, G. Petekidis, M. E. Cates, and W. C. K. Poon, *Phys. Rev. Lett.* **105**, 268301 (2010).
- [65] L. Bécu, S. Manneville, and A. Colin, *Phys. Rev. Lett.* **96**, 138302 (2006).